scientific reports

OPEN

Design of a parameter self-tuning PID controller based on an ER-SLP for a variable-frequency air compressor in a rapid deballasting system

Shouwen Pang✉ & Jingxin Zhou

The rapid deballasting system is a critical component of the semisubmersible lifting and decommissioning platform of offshore oilfield platforms. During operation, compressed air is injected into the column side ballast chamber by an air compressor to maintain the stability of the platform. The objective of this study is to address the issues of high energy consumption, backward control methods, and low efficiency in power frequency air compressors. To this end, frequency conversion is carried out via simulation. A novel fractional PID controller design, which is based on evidential reasoning (ER) and sequential linear programming (SLP) methodologies, is proposed. The proposed algorithm is evaluated in comparison with power frequency control, a traditional PID controller, and a fractional PID controller within the context of a simulation model established within the Simulink environment. The evaluation is conducted under typical working conditions. The results of the simulation demonstrate that the ER fractional PID controller is more effective in balancing energy consumption and operation time during the operational process and exhibits superior control performance. Specifically, compared to traditional PID and fractional PID controllers, the ER-SLP-based controller achieves 7.2% energy savings over power frequency control while reducing task completion time by 4.7% versus traditional PID. Additionally, it demonstrates enhanced robustness and adaptability under dynamic conditions, addressing pressure fluctuations and computational efficiency challenges in existing methods. This work provides a data-driven, real-time optimization framework for industrial control systems requiring energy-time trade-offs.

Keywords Energy-saving transformation of an air compressor, Fractional PID, Evidential reasoning rule, Sequential linear programming

The air compressor in the rapid deballasting system represents a significant energy consumer in the context of semisubmersible lifting and dismantling platforms. The primary function of the apparatus is to generate compressed air, which is then used to rapidly deball the ballast tank on the lifting side. This allows for the adjustment of the stability of the platform in a relatively short time. Nevertheless, the air compressors utilized in the rapid deballasting system of semisubmersible lifting and dismantling platforms are power frequency air compressors, which present several challenges. These include high energy consumption, low efficiency, and inflexible control modes. The objective of this field of study is to determine the optimal balance between the energy consumption of the air compressor and its operational time, with the aim of ensuring normal operation within the specified time frame.

In the field of energy-saving control of air compressors, R. Saidur's research[1] focused primarily on the investigation of energy consumption in air compressors employing energy-saving strategies. Additionally, Saidur conducted retrofitting of power frequency air compressors with variable-frequency air compressors, with the objective of increasing energy efficiency. Variable-frequency air compressors typically employ PID controllers to facilitate the automatic adjustment of compressor operating modes and the balancing of operational time across all compressors. In light of the pivotal role played by parameter tuning in the operation of PID controllers,

School of Navigation and Shipping, Shan Dong Jiao Tong University, Weihai 264200, Shandong, China. ✉email: 35639864@qq.com

particularly in meeting the demands of sophisticated industrial control systems, experts in this field have been engaged in the pursuit of more effective tuning methodologies for PID controller parameters. This has led to the development of numerous established tuning techniques, including the ZN and ISTE methods. The aforementioned methods establish a model that describes the nonlinear relationship between control system variables (including the given input, actual output, deviation, etc.) and PID controller parameters (including the proportional coefficient Kp, integral coefficient Ki, differential coefficient Kd), which can effectively control the actual system.However, existing intelligent PID methods (e.g., fuzzy PID) rely heavily on expert knowledge and fixed rule bases, leading to limited adaptability in highly nonlinear systems like rapid deballasting. In contrast, our ER-SLP fractional PID uniquely combines data-driven ER inference with online parameter optimization, eliminating the need for prior expert rules while enhancing real-time adaptability. Furthermore, they have been shown to lack the requisite adaptability and robustness, which significantly diminishes their effectiveness. As a result of extensive research in the field of intelligent control, numerous intelligent control technologies have reached a high level of maturity and are now being employed in a variety of fields. Some experts and scholars have proposed a synthesis of the intelligent control method with the traditional PID control method, resulting in the introduction of a variety of new intelligent PID (IPID) control methods. This method allows for the separation of knowledge acquisition and knowledge processing and is capable of processing incomplete and uncertain knowledge. However, there are also some issues that require further attention, including (1) how to obtain sufficient expert knowledge and transform it into a form that can be readily used; (2) how to resolve the problem of rule combination explosion caused by a vast knowledge base; and (3) how to enhance the online learning capacity of the expert system, ensuring the completeness and adaptability of the rule base. The evidential reasoning (ER) rule, as proposed by Yang, is an algorithmic approach based on machine learning. The ER rule offers three key advantages. First, it employs a data-driven approach to describe the relationship between the output and input parameters rather than relying on empirical formulas. Second, the ER rule assigns the remaining beliefs resulting from the reliability discount to the power set. The complete set represents global ignorance, which is an element in the power set. Consequently, the utilization of the ER rule is more effective than alternative methodologies in addressing the challenge of inferring output parameters from incomplete data samples. Additionally, the physical interpretation of each parameter in the ER rule is more straightforward than that of neural networks. The parameters may be modified according to the specific requirements of the intended application[2].

Related work

The energy-saving control of air compressors has garnered significant attention in industrial applications. Traditional PID controllers remain widely adopted due to their simplicity and reliability, yet their fixed parameters often lead to suboptimal performance in nonlinear systems like rapid deballasting. Recent advancements in intelligent PID tuning methodologies aim to address these limitations.

Fuzzy PID Control: Kim et al.[3] proposed a fuzzy PID controller for variable-frequency air compressors, leveraging expert-defined rules to adjust parameters dynamically. While effective in reducing overshoot, its reliance on empirical knowledge limits adaptability in complex scenarios with incomplete data.

Deep Learning-Based Optimization: Zhang et al.[4] integrated deep reinforcement learning (DRL) with PID control, achieving energy savings of 15% in HVAC systems. However, the high computational cost of DRL impedes real-time deployment in fast-response systems like deballasting.

Evidential Reasoning in Control: Recent studies by Xiao et al.[5] applied ER rules to multi-sensor fusion in robotic systems, demonstrating robustness under uncertain inputs. Their work highlights ER's potential for data-driven parameter inference but lacks integration with online optimization frameworks.

SLP in Real-Time Systems: Lamberti et al.[6] utilized SLP for structural optimization, showcasing its efficiency in iterative parameter tuning. Yet, its application to dynamic control systems remains underexplored.

Variable-Frequency Compressor Studies: Kong et al.retrofitted power-frequency compressors with variable-frequency drives, achieving 12% energy savings but noted persistent pressure fluctuations due to static PID parameters.

Compared to existing methods, our ER-SLP fractional PID uniquely combines ER's data-driven reasoning with SLP's real-time optimization, eliminating dependency on prior expert rules while enhancing adaptability. This hybrid approach addresses gaps in energy-time trade-offs, as evidenced by the 7.2% energy saving and reduced operational time in simulations.

Please refer to the remainder of the paper, which is detailed below. Section 2 presents an overview of the operational principles underlying the rapid deballasting system. Furthermore, a combined air compressor unit cluster control strategy based on a variable frequency and power frequency is proposed. Section 3 presents the proposed fractional PID controller, which is designed to enhance the rapidity of the air compressors while simultaneously conserving energy. The ER fractional PID controller was designed with the objective of achieving real-time control of the fractional PID under different working conditions. In Sect. 4, the theories of the ER rule and the SLP-optimized model parameters of the ER rule are explored. In Sect. 5, a model of the rapid deballasting process is constructed within the Simulink environment. The control performances of the four control types are compared. The findings of this study are presented in Sect. 6.

Working principle of the rapid deballasting system

The present study focuses on the "Serooskerke" platform as the primary research object[6]. The configuration of the platform is illustrated in Fig. 1. The platform is divided into two independent pontoons at its base. The left side is the outrigger pontoon, whereas the right side is the main pontoon. Each pontoon is supported by two columns located above it. The upper deck is supported by four columns, and two mast cranes, with a lifting

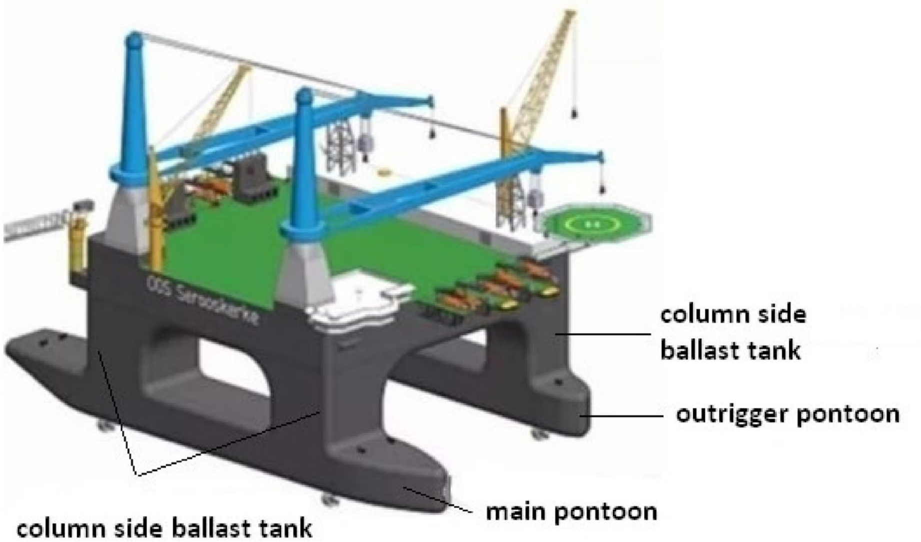

Fig. 1. "Serooskerke" semisubmersible lifting and dismantling platform.

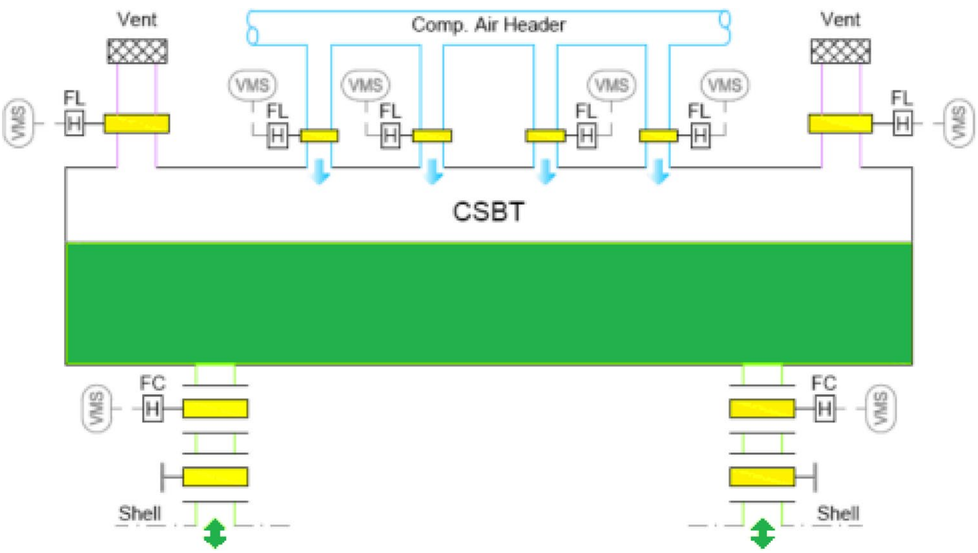

Fig. 2. Schematic diagram of the column-side ballast tank structure.

capacity of 2,200 tons, are situated on the side of the main pontoon. A column side ballast tank (CSBT) is located within each of the four columns, providing a rapid means of deballasting. The volumes of the two-column side ballast tanks (CSBTMP#1/2) on the main pontoon side are 2193.8 m^3 and 2188.0 m^3. With respect to the outrigger pontoon, the volumes of the two column side ballast tanks (CSBTOP#1/2) are 1570.7 m^3 and 1563.6 m^3. The platform is equipped with three air compressors, which are utilized for rapid discharging, and one additional compressor that serves as a backup.

The column side ballast tank is an important part of the rapid deballasting system[7]. Its design is shown in Fig. 2. There are four air intake valves and two vent valves at the top and two sea valves at the bottom, which are connected directly to the outboard engine. The operation of the valves is controlled by the vessel management system (VMS). The air manifold is connected to the four side-mounted ballast tanks, and the compressed air flows from the air manifold to the ballast tanks through intake valves as required by the VMS. In the rapid deballasting system, three air compressors are used in succession during the lifting operation, with one air compressor on standby. Once started, the air compressors remain in loading or unloading mode until the lifting operation is completed. In the original rapid deballasting system, the power frequency air compressor unit uses a step control strategy, as shown in Fig. 3. Step control means that the charging and discharging pressures of each air compressor are distributed in steps, and the charging and discharging pressures of two adjacent compressors are increased. The loading/unloading pressures of air compressors A, B and C are 0.14/0.17 MPa, 0.17/0.20 MPa,

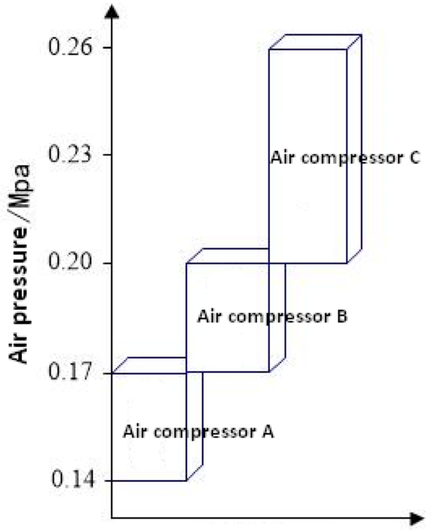

Fig. 3. Power frequency step control diagram.

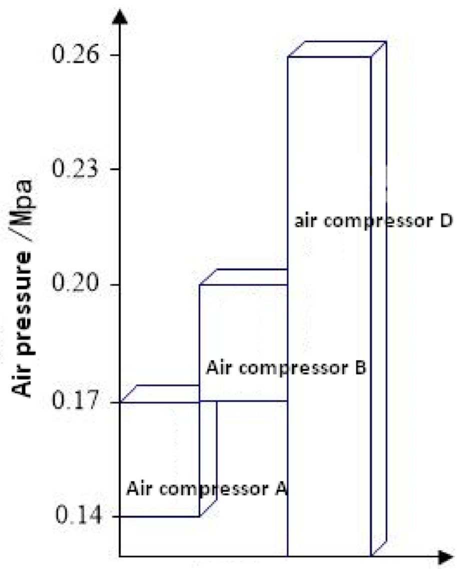

Fig. 4. Combined power-frequency-variable-frequency control diagram.

and 0.20/0.26 MPa, respectively. The rated power is 630 kW, the rated displacement is 8391.6 m^3/h, and the discharge pressure is 0.26 MPa.

Under lifting conditions, the step-controlled power frequency air compressor is always in the loading and unloading state after starting, and the unloading state still consumes a large amount of energy, which also results in large air pressure fluctuations. The step-controlled air compressor is then converted into a variable-speed air compressor with the same rated power and the same rated displacement. This is because the displacement of the variable-frequency air compressor changes as the frequency changes, reducing air pressure fluctuations in the air receiver and column-side ballast tank. After the frequency conversion transformation, the pressure difference of the last stage of the stepped air compressors is reduced.

In this case study, fixed-frequency air compressor C is converted to variable-frequency air compressor D, which is consistent with the cluster control strategy for the fixed-frequency/variable-frequency combined air compressor unit. The retrofit plan is shown in Fig. 4. The fixed-frequency air compressors A and B remain unchanged, and the variable-frequency air compressor D has the same rated power, rated displacement and discharge pressure as air compressors A and B.Key System Parameters is shown in (Table 1).

Parameter	Value
Rated power	630 kW
Rated displacement	8391.6 m^3/h
Target pressure	0.26 MPa
Initial boom angle	73°

Table 1. Key system parameters.

Fractional PID controller

The air compressor is the largest energy consumer in the rapid deballasting system. Variable frequency control can reduce the energy consumption of compressors. Generally, the PID controller can control the power supply frequency of the variable-frequency air compressor, thereby controlling the displacement of the air compressors. Unlike the traditional PID controller, the fractional PID controller adds an index to the integral parameter I and the differential parameter D, namely, PIλDμ. Mathematically, the exponential function is also called the "explosive" function, which provides faster response.

Theory of fractional calculus

Fractional calculus is the extension and expansion of integer calculus[6], and its order can be any complex number. The operators of fractional calculus can be expressed as:

$$ {}_{a}D_{t}^{\alpha} = \begin{cases} \frac{d^{\alpha}}{dt^{\alpha}}, & Re\left(\alpha\right) > 0 \\ 1, & Re\left(\alpha\right) = 0 \\ \int \left(d\tau\right)^{\alpha}, & Re\left(\alpha\right) < 0 \end{cases} \tag{1} $$

In the formula, a and t are the upper and lower limits of the calculus, α is any complex number, and $Re\left(\alpha\right)$ is the real part of α. However, the orders of magnitude discussed in this chapter are all real numbers.

Fractional PID controller

The differential equation of the fractional PID controller is similar to that of the traditional PID controller:

$$ u\left(t\right) = Kpe\left(t\right) + KiD^{-\lambda}e\left(t\right) + KdD^{\mu}e\left(t\right) \tag{2} $$

where $De\left(t\right)$ is the fractional operator defined by Caputo. The fractional PID controller has five controller parameters: Kp, Ki, Kd, λ and μ. Transforming the time-domain expression of the fractional calculus via the Laplace transform yields the following formula:

$$ L\left\{{}_{a}{}^{c}D_{t}^{\alpha}f\left(t\right)\right\} = s^{\alpha}F\left(s\right) - \sum_{k=0}^{N-1} S^{\alpha-k-1}f^{k}\left(0\right) \tag{3} $$

Under zero initial conditions, the above formula can be expressed as:

$$ L\left\{{}_{a}{}^{c}D_{t}^{\alpha}f\left(t\right)\right\} = s^{\alpha}F\left(s\right) \tag{4} $$

The transfer function of the fractional PID controller is as follows:

$$ Gc\left(s\right) = Kp + \frac{Ki}{s^{\lambda}} + Kds^{\mu}, \left(\lambda, \mu > 0\right) \tag{5} $$

where λ and μ are the order of the integral coefficient and the order of the differential coefficient of the controller, respectively, and the value is a nonnegative real number, which expands the adjustable range of integration and differentiation and improves the control accuracy of the fractional controller. At the same time, however, the parameter tuning of the controller becomes more difficult.

Recent advancements in fractional-order control have demonstrated improved robustness in nonlinear systems. For instance, Tepljakov et al. [7] proposed a systematic tuning framework for fractional PID controllers using frequency-domain optimization, which aligns with our approach of dynamic parameter adaptation.

ER fractional PID controller design

The relationship between the input parameters and the control parameters of the controller is modeled according to the ER rule to achieve real-time control of the fractional PID under different operating conditions in the ER fractional PID controller. The five parameters of the controller are set[8]. The control system diagram is shown in Fig. 5.

The air pressure in the ballast tank, the target air pressure and the pressure deviation are used as the three input parameters of the ER rule, and the five parameters designated ΔKp, ΔKi, ΔKd, $\Delta\lambda$, and $\Delta\mu$ are the output parameters used as the control parameters of the controller. The initial domain of $\Delta\lambda$, $\Delta\mu$ is $[-0.1, 0.1]$; the initial domain of the remaining parameters is $[-3, 3]$; and the weight, reliability and parameter range in the ER algorithm are all optimized by the SLP optimization algorithm. The overall modeling and reasoning process is as follows:

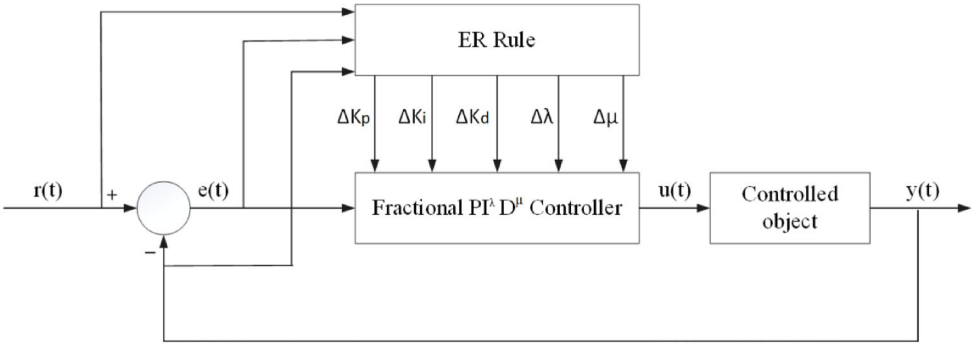

Fig. 5. Block diagram of the ER fractional PID control system.

(1) Evidential reasoning models are built on the basis of qualitative knowledge and quantitative data, and the model parameters are initialized. The empirical sample set is obtained through the simulation model, and the initial reference evidence matrices $REMKp$, $REMKi$, $REMKd$, $REMVi$ and $REMVd$ of Kp, Ki, Kd, Vi (λ), and Vd (μ) are generated on this basis.
(2) The input sample $X(k) = [f1(k),\ f2(k),\ f3(k)]$ is obtained online at the k-th moment and substituted into $REMKp$, $REMKi$, $REMKd$, $REMVi$and $REMVd$, and the evidence is activated (e_1^{Kp}, e_2^{Kp}, e_3^{Kp}, e_1^{Ki}, e_2^{Ki}, e_3^{Ki}, e_1^{Kd}, e_2^{Kd}, e_3^{Kd}, e_1^{Vi}, e_2^{Vi}, e_3^{Vi}, e_1^{Vd}, e_2^{Vd}, e_3^{Vd}). The ER rule is used to fuse the evidence of activation to generate estimates of the PID controller parameters $Kp(k)$, $Ki(k)$, $Kd(k)$, $Vi(k)$, and $Vd(k)$ corresponding to the parameters of the PID controller Kp, Ki, Kd, Vi and Vd to obtain the corresponding outputs.
(3) Determine the optimized objective function of the ER-PID controller and the model parameters to be fine-tuned at time k. The weight, reliability and parameter range in the ER algorithm are optimized and updated by the SLP algorithm at time k.
(4) The optimized parameters at time k are used as the initial parameters of the model at time $k+1$. Then, returning to (2), the inference process is performed at time $k+1$, and the above processes are repeated until the stopping criteria are satisfied. The tuning parameter expression is as follows:

$$\begin{cases} Kp = Kp_0 + \Delta Kp \\ Ki = Ki_0 + \Delta Ki \\ Kd = Kd_0 + \Delta Kd \\ \lambda = \lambda_0 + \Delta \lambda \\ \mu = \mu_0 + \Delta \mu \end{cases} \tag{6}$$

In the formula, Kp_0, Ki_0, Kd_0, λ_0, and μ_0 are the initial setting values of the controller parameters after preliminary turning, which are 1242.6, 0.09, 3000, 0.85, and 0.99, respectively, and ΔKp, ΔKi, ΔKd, $\Delta\lambda$, and $\Delta\mu$ are increments obtained after ER rule optimization.

In summary, the MATLAB/Simulink module is used to construct a fractional PID control system, and the relationships between the input parameters and output parameters are modeled via the ER rule. Finally, the parameters of the ER rule are optimized in real time according to the SLP method.

In this work, the air pressure in the ballast tank, the target air pressure and the pressure deviation are used as the three input parameters of the ER rule, and the five parameters Kp, Ki, Kd, Vi (λ), and Vd (μ) are the output parameters. The matrix model of the relationship between the three input parameters and the five output parameters is as follows:

(1) The data sample set generated by the simulation model can be expressed as follows: $S = \{[f_1(k), f_2(k), Kp(k), Ki(k), Kd(k), Vi(k), Vd(k)] | k = 1,2,\ldots, M\}$, where $M \geq$ 10000. The complete dataset can be classified into five distinct subsets, corresponding to PID controller parameters Kp, Ki, Kd, Vi and Vd. To construct an REM that describes the relationship between one of the output variables Kp, Ki, Kd, Vi and Vd andthe input variable f_i, three subdata sets are used. The construction of $REMKp$ is described in detail in steps 2 and 3. The development of other matrices is analogous to that of $REMKp$.
(2) As the reference values of the input $A_i (i = 1,2,3)$ and the reference values of the output D^p can be modified, the initial values of A_i and D^p of Kp are established by experts or assigned randomly. The relationship between f_i and Kp is transformed into a relationship between the output reference value and the input reference value. $A_i = \{A_1^i, \ldots, A_t^i, \ldots, A_{T_i}^i | i = 1,2; t = 1,2,\ldots, T_i\}$, A_i is the reference value set of f_i, $D^p = \{D_1^p, \ldots, D_s^p, \ldots, D_N^p | s = 1,2,\ldots N\}$, and D^p is the reference value set of Kp. In this context, p represents the proportional component of the PID controller, and T_i and s are the numbers of reference values of f_i and Kp, respectively. These reference values are restricted to $A_1^i < A_2^i < \cdots < A_{T_i}^i$, where $D_1^p < D_2^p < \cdots < D_N^p$. The similarity distributions of the input variables $f_i(k)$ and A_i are the reference values of $f_i(k)$ at time k as follows: $S_p(f_i(k)) = \{(A_t^i, \alpha_{i,t}) | t = 1,2,\ldots, T_i; i = 1,2\}$. $\alpha_{i,t}$ can quantify the level of similarity between the input variable $f_i(k)$ and the input reference value A_t^i, which is calculated via a piecewise linear function in Eq. (7):

f_i / Kp	A_1^i	...	A_t^i	...	$A_{T_i}^i$	Total
D_1^p	$a_{1,1}$	...	$a_{1,t}$	...	a_{1,T_i}	δ_1
⋮	⋮	⋮	⋮	⋮	⋮	⋮
D_s^p	$a_{s,1}$	...	$a_{s,t}$	...	a_{s,T_i}	δ_s
⋮	⋮	⋮	⋮	⋮	⋮	⋮
D_N^p	$a_{N,1}$	...	$a_{N,t}$	...	a_{N,T_i}	δ_N
Total	η_1	...	η_t	...	η_{T_i}	M

Table 2. The similarity matrix between the sample pair ($fi\,(k)$, $Kp\,(k)$) and its reference value.

f_i	$e_1^{i,p}$	...	$e_t^{i,p}$	...	$e_{T_i}^{i,p}$
Kp	A_1^i	...	A_t^i	...	$A_{T_i}^i$
D_1^p	$\beta_{1,1}^{i,p}$	...	$\beta_{1,t}^{i,p}$	...	$\beta_{1,T_i}^{i,p}$
⋮	⋮	⋮	⋮	⋮	⋮
D_s^p	$\beta_{s,1}^{i,p}$	...	$\beta_{s,t}^{i,p}$	...	$\beta_{s,T_i}^{i.p}$
⋮	⋮	⋮	⋮	⋮	⋮
D_N^p	$\beta_{N,1}^{i,p}$	...	$\beta_{N,t}^{i,p}$	...	$\beta_{N,T_i}^{i,p}$

Table 3. The relationship matrix of fi.

$$\begin{cases} \alpha_{i,t} = \frac{A_{t+1}^i - f_i(k)}{A_{t+1}^i - A_t^i}; \alpha_{i,t+1} = \frac{f_i(k) - A_t^i}{A_{t+1}^i - A_t^i} & A_t^i \le f_i(k) \le A_{t+1}^i \\ \alpha_{i,1} = 1; \alpha_{i,t} = 0(t \ne 1) & f_i(k) \le A_1^i \\ \alpha_{i,T_i} = 1; \alpha_{i,t} = 0(t \ne T_i) & f_i(k) \ge A_{T_i}^i \end{cases} \tag{7}$$

Similarly, the output variable and its analogous distribution can be expressed as $S_O\,(Kp(k)) = \{(D_s^p, \gamma_s^p) |\, s = 1,2,\ldots, N\}$, and γ_s^p can be represented as the output variable $Kp\,(k)$. The similarity with its reference value D_s^p is calculated via a piecewise linear function, as expressed in Eq. (8):

$$\begin{cases} \gamma_s^p = \frac{D_{s+1}^p - K_p(k)}{D_{s+1}^p - D_s^p}; \gamma_{s+1}^p = \frac{K_p(k) - D_s^p}{D_{s+1}^p - D_s^p} & D_s^p \le f_i(k) \le D_{s+1}^p \\ \gamma_1^p = 1; \gamma_s^p = 0(s \ne 1) & K_p(k) \le D_1^p \\ \gamma_N^p = 1; \gamma_s^p = 0(s \ne N) & K_p(k) \ge D_N^p \end{cases} \tag{8}$$

(3) Integrate the original samples $(f_i(k),\, Kp(k))$ into the similarity distribution $(\alpha_{i,t}\gamma_s^p, \alpha_{i,t+1}\gamma_s^p, \alpha_{i,t}\gamma_{s+1}^p, \alpha_{i,t+1}\gamma_{s+1}^p)$, where $\alpha_{i,t}\gamma_s^p$ represents the input $f_i\,(k)$ and its reference value A_t^i, the comprehensive degree of matching between the output $Kp\,(k)$ and the output reference value D_s^p at the same time. The integration similarity is employed to describe all samples within the dataset, indicating the degree of correspondence between the input reference values and the output reference values. The similarity matrix is presented in Table 2 for reference.

In Table 2, $a_{s,t}$ represents the sum of the total similarity between the sample pair $(f_i(k),\, Kp(k))$ and its reference values A_t^i and D_s^p. We can also see that $\eta_t = \sum_{s=1}^N a_{s,t}$ and $\delta_s = \sum_{t=1}^{T_i} a_{s,t}$; moreover, they satisfy $\sum_{s=1}^N \delta_s = \sum_{t=1}^{T_i} \eta_t = M$. As indicated in Table 2, the probability distributions of $f_i\,(k)$, A_t^i, $Kp\,(k)$ and D_s^p can be represented by the following formula (9):

$$c_{s,t} = p\left(A_t^i \middle| D_s^p\right) = \frac{a_{s,t}}{\delta_s} \tag{9}$$

In Table 3, the initial $REMKp$ shows the mapping between the output Kp and the input f_i . $e_t^{i,p} = [\beta_{1,t}^{i,p}, \ldots, \beta_{s,t}^{i,p}, \ldots, \beta_{N,t}^{i,p}]$ indicates the evidence corresponding to input f_i and their reference value A_t^i. $\beta_{s,t}^{i,P}$ represents the confidence that $Kp\,(k)$ and D_s^p match under the evidence $e_t^{i,p}$ and satisfies $\sum_{s=1}^N \beta_{s,t}^{i,p} = 1$. The normalized likelihood function value $c_{s,t}$ can be used to calculate $\beta_{s,t}^{i,p}$ via formula (10):

$$\beta_{s,t}^{i,p} = \frac{c_{s,t}}{\sum_{k=1}^{N} c_{k,j}} \tag{10}$$

Algorithm principle

Evidential reasoning rule

The ER rule serves to distinguish between the concepts of evidence reliability and evidence importance[9]. Furthermore, the ER rule extends the traditional D-S evidence theory and ER algorithm in a more comprehensive manner, offering a novel perspective and a more rigorous logical reasoning system[10]. The particular principle can be stated as follows:

Let us assume that Θ is a recognition framework composed of N mutually exclusive elements h_1, h_2, $h_3 ... h_N$. Θ and the subsets it contains form the set represented by P_θ. The belief distribution of evidence e_j is shown in formula (11):

$$e_j = \{(\theta, p_{\theta,j}) | \forall \theta \subseteq \Theta, \sum_{\theta \subseteq \Theta} p_{\theta,j} = 1\} \tag{11}$$

where $p_{\theta,j}$ represents the degree to which e_j supports the θ proposition, which can be defined as a belief function or a belief distribution. θ is any element of any nonempty set. In the ER rule, e_j are represented by the credibility r_j and the weight w_j. r_j are the objective and intrinsic attributes of the evidence e_j, which objectively reflects the ability of a source that generates the e_j to estimate parameters or solve problems. Nevertheless, the significance of evidence is subjective and contingent upon the experience and perspective of the user. When different sources obtain different evidence, the importance of one piece of evidence is reflected by the weight of the evidence w_j. The reliability distribution and the weight distribution of evidence are illustrated in formula (12):

$$m_j = \{(\theta, \tilde{m}_{\theta,j}), \forall \theta \subseteq \Theta; (P(\Theta), \tilde{m}_{P(\Theta),j})\} \tag{12}$$

where $\tilde{m}_{\theta,j}$ represents the degree to which e_j supports proposition θ, which is a factor of the reliability and weight of the evidence e_j. $\tilde{m}_{\theta,j}$ can be calculated according to formula (13).

$$\tilde{m}_{\theta,j} = \begin{cases} 0 & \theta = \varphi \\ c_{rw,j} m_{\theta,j} & \theta \subseteq \Theta, \theta \neq \varphi \\ c_{rw,j}(1 - r_j) & \theta = P(\Theta) \end{cases} \tag{13}$$

where $m_{\theta,j} = w_j p_{\theta,j}$, $c_{rw,j} = 1/(1 + w_j - r_j)$ is the normalization factor, and when $\sum_{\theta \subseteq \Theta} p_{\theta,j} = 1$, $\sum_{\theta \subseteq \Theta} \tilde{m}_{\theta,j} + \tilde{m}_{P(\Theta),j} = 1$. The remaining support of the ER rule $(1 - r_j)$ will be reallocated to the set $P(\theta)$ that replaces the recognition framework mentioned by formula (11).

When there are two independent pieces of evidence supporting proposition θ, the joint confidence $p_{\theta,e(2)}$ of the θ proposition supported by the two independent pieces of evidence e_1 and e_2 is defined as:

$$p_{\theta,e(2)} = \begin{cases} 0 & \theta = \varphi \\ \frac{\tilde{m}_{\theta,e(2)}}{\sum_{D \subseteq \Theta} \tilde{m}_{D,e(2)}} & \theta \subseteq \Theta, \theta \neq \varphi \end{cases} \tag{14}$$

$$\tilde{m}_{\theta,e(2)} = [(1 - r_2) m_{\theta,1} + (1 - r_1) m_{\theta,2}] + \sum_{B \cap C = \theta} m_{B,1} m_{C,2} \forall \theta \subseteq \Theta \tag{15}$$

When L pieces of independent evidence e_j $(j = 1, 2, ..., L)$ are fused, the recurrence formula is as follows:

$$\tilde{m}_{\theta,e(i)} = \left[(1 - r_i) m_{\theta,e(i-1)} + m_{P(\Theta),e(i-1)} m_{\theta,i}\right] + \sum_{B \cap C = \theta} m_{B,e(i-1)} m_{C,i} \forall \theta \subseteq \Theta \tag{16}$$

$$\tilde{m}_{P(\Theta),e(i)} = (1 - r_i) m_{P(\Theta),e(i-1)} \tag{17}$$

Taking the control system in Fig. 5 as an example, the input parameters (tank air pressure, target air pressure, pressure deviation) activate the corresponding evidences (e.g., e_1^Kp, e_2^Kp) through ER rules.The output parameters (ΔKp, ΔKi, etc.) dynamically adjust the controller through the fusion process of Eqs. (14)-(17) for real-time optimisation.For example, the ER rule automatically reduces the Kp gain to minimise overshoot when the air pressure in the tank approaches the target value.

The integration of ER rules with real-time optimization has been further validated in industrial applications. As highlighted by Liu et al.[11], ER-based methods significantly enhance decision-making under uncertainty in multi-sensor systems, supporting the adaptability of our methodology.

Sequential linear programming

In the majority of studies examining the ER rule, the model parameters are optimized offline through the utilization of training sample sets. This is a global optimization method that requires a sufficient number of training samples to function effectively. The lack of sufficient data samples may result in the adjustment parameters diverging from their optimal values, thereby reducing the accuracy of the control process. To circumvent this issue, this paper employs the SLP optimization algorithm to facilitate the local and dynamic optimization of the model parameters. This entails the optimization of solely those parameters pertaining to the activation evidence[12].

As the name suggests, sequential linear programming (SLP) is an iterative optimization method that is achieved by linearizing any nonlinear terms (including cost functions and constraints) around the current solution point[13]. The solution subsequently addresses the nonlinear issue by identifying a new point until the predefined stopping criterion is met. The sequential linear programming method comprises the following principal stages:

(1) Linearize the nonlinear objective function.

The objective function ξ(P(k)) and its constraints are expanded by a Taylor series so that the objective function can be approximated to the linearized function of formula (18).

$$\xi\ (P(k)) \approx \xi\ (P_0(k)) + \xi\prime\ (P_0(k))\,(P(k) - P_0(k)) \tag{18}$$

In formula (18), $\xi\ (P_0(k))$ represents the objective function value corresponding to $P_0\,(k)$, $P_0\,(k)$ represents the initial point, and $\xi\prime\ (P_0(k))$ represents the derivative of the objective function corresponding to $P_0\,(k)$. The nonlinear objective function is linearized, thereby transforming the nonlinear optimization problem into a linear programming problem.

(2) Determine the range of the optimization parameters.

In the SLP algorithm, the selection of the variation range of the optimization parameter is highly beneficial for optimizing performance. It has been demonstrated that a variation range that is either too large or too small results in a reduction in the accuracy of the optimization. The upper bound of the optimization parameter, designated UB(P), is determined through the application of Eqs. (19) and (20). The initial movement limit of each parameter in P is set to 10% of its upper limit.

$$UB\,(w_i) = 1, i = 1,2,3 \tag{19}$$

$$UB\left(\beta_{s,t}^{\,i,Z}\right) = 1, i = 1,2,3, s = 1,2,\ldots,N; t = 1,2,\ldots,T_i; Z = 1,2,3,4,5 \tag{20}$$

where w, β represents the weight and confidence, i and Z represent the numbers of input variables and output variables, respectively, and t and s represent the numbers of reference values of the input variables and output variables, respectively.

(3) Sequential linear programming is used to search for the optimal solution.

In step 1 and step 2, the linearization function $\xi\ (P(k))$ and the variation range of the optimized parameters under the condition of determining the initial point $P_0\,(k)$ are obtained. Concurrently, the search space is defined in accordance with the known initial point and motion limit, and the search process is conducted through the utilization of the linear programming method. In the event that the constructed search space intersects with the linearized feasible solution space and is found to be empty, it is necessary to expand the search space by increasing the movement limit. Conversely, in the event of an intersection point being identified, the optimal solution to the linear programming problem is determined at that point[14]. The optimal solution is subsequently taken as a new base point, and the initial nonlinear optimization problem is relinearized. This marks the commencement of an iterative process, whereby the optimization is executed until a specific stopping condition is met.

(4) SLP optimization stopping criterion.

The optimization of the SLP is contingent upon the satisfaction of two criteria. Upon the fulfillment of any one of the aforementioned criteria, the iterative process is terminated. The two criteria are as follows: (a) the displacement of all the parameters must be significantly small; (b) in two adjacent iterations, there must be no significant change in the value of the optimization parameter or the objective function value.

Modern adaptations of SLP for dynamic systems, such as the work by Zhang and Li[15], emphasize its efficiency in real-time parameter tuning, reinforcing our choice of SLP for online optimization.

Simulation

Typical working conditions defined in this paper include: twin cranes working together to lift a 4200 tonne load, initial boom angle of 73°, the main float side as the lift side, and target pressure of 0.26 MPa. A simulation model of the rapid deballasting system is constructed for each control strategy, including the power frequency, traditional PID, fractional PID and ER fractional PID. A schematic diagram of the simulation model is provided in Fig. 6. The simulation model is calibrated by comparing the historical data of the actual platform (e.g. the energy consumption record of a 4200-tonne lifting task in 2022), and the validation results show that the maximum error of the dynamic response of the pressure and level is less than 5%, which meets the engineering accuracy requirements.

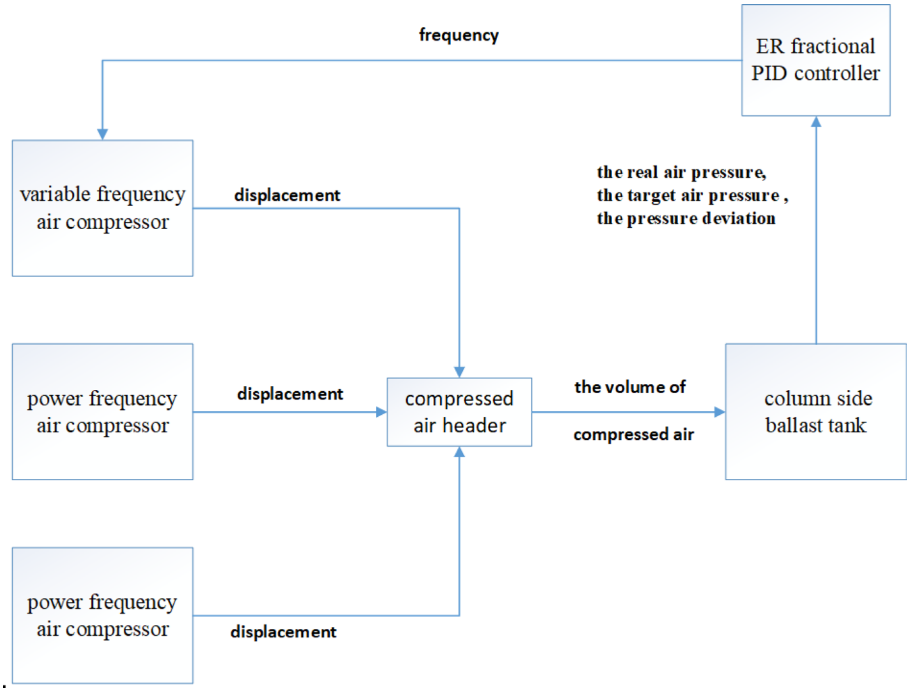

Fig. 6. Schematic diagram of the simulation model based on the ER fractional PID.

-	CSBTMP#1	CSBTMP#2	CSBT OP#1	CSBT OP#2
Initial volume/m^3	2116	2111	47	46
Final volume/m^3	278	279	1462	1457

Table 4. Changes in the seawater volume in the column ballast tanks.

Recent studies on variable-frequency compressors, such as those by Wang et al.[16], highlight energy-saving potentials through adaptive control, corroborating our simulation results on energy-time trade-offs.

The double-crane tandem lifting 4200T configuration was selected for simulation experimentation and comparison. The hook load radius of the boom is 22.1 m, the initial angle of the boom is 73°, and the main pontoon is the lifting side. In the event of lifting, the two-column side ballast tanks on the main pontoon side (CSBTMP #1/2) utilize compressed air to discharge the load, whereas the two-column side ballast tanks (CSBTOP #1/2) on the outrigger pontoon side are ballasted by gravity water injection, thereby ensuring the stability of the platform's center of gravity[17]. The changes in the volume of seawater in the ballast tanks of the four columns under lifting conditions, as indicated by the platform stability data provided by the China Merchants Heavy Industry Group (Jiangsu), are presented in Table 4.

As illustrated in Fig. 7, the air compressor initiates the inflow of air into the cabin from zero time. Concurrently, the subsea valve is opened to discharge, and the water level in the ballast tank undergoes a change, as illustrated in Fig. 8. Upon reaching the target water level corresponding to the final volume indicated in Table 3, the subsea valve is closed, thereby completing the lifting condition.

By combining the data from Figs. 7 and 8, it is possible to ascertain the completion time of the working conditions under the four control modes. Similarly, the energy consumption under these four control modes can be calculated via the data from Fig. 9. The control indicators are presented in Table 5 below.

A comparison of the four control methods presented in Table 5 reveals that the power frequency control method requires the shortest amount of time to complete the lifting task but also results in the highest energy consumption. The traditional PID control method results in the lowest energy consumption but also the longest completion time for lifting tasks.Compared to the conventional PID, the ER fractional-order PID increased the energy consumption by 5.6% (553.5 vs. 52. 4.0 kW-h) but reduced the task time by 4.7% (2,169 vs. 2,276 s), validating its ability to balance energy efficiency with speed. Fractional PID and ER fractional PID control demonstrate performance characteristics that are intermediate to these two extremes. Compared with fractional PID control, the implementation of ER fractional PID control results in a slight increase in energy consumption. However, this approach allows for the completion of the task in a shorter time frame. To reduce energy consumption and mitigate pressure fluctuations, minimizing the discharge time is imperative. It is therefore recommended that the ER fractional PID controller be employed for the frequency conversion transformation of the rapid deballasting system.

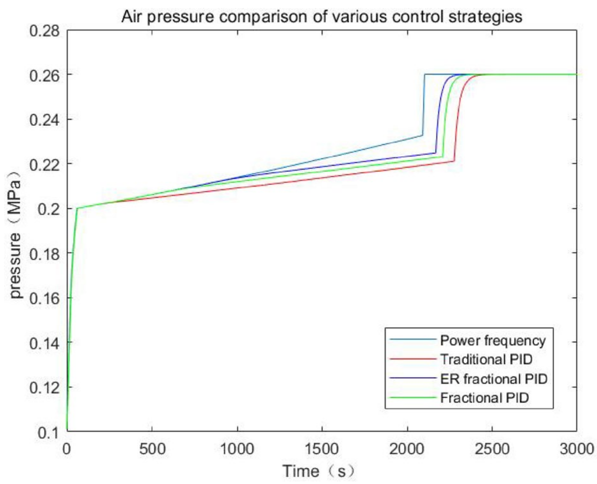

Fig. 7. Air pressure comparison of various control strategies.

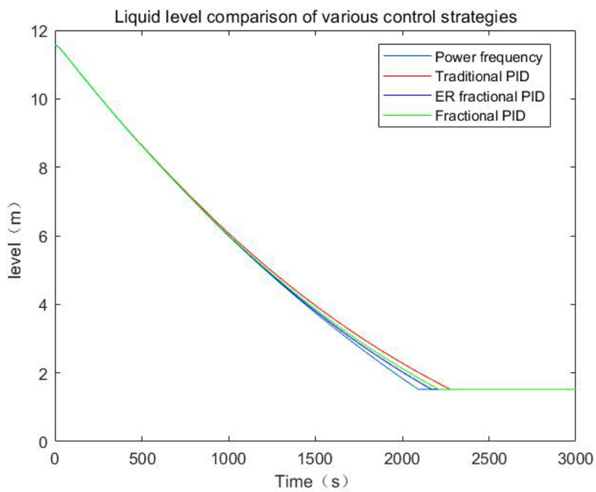

Fig. 8. Liquid level comparison of various control strategies.

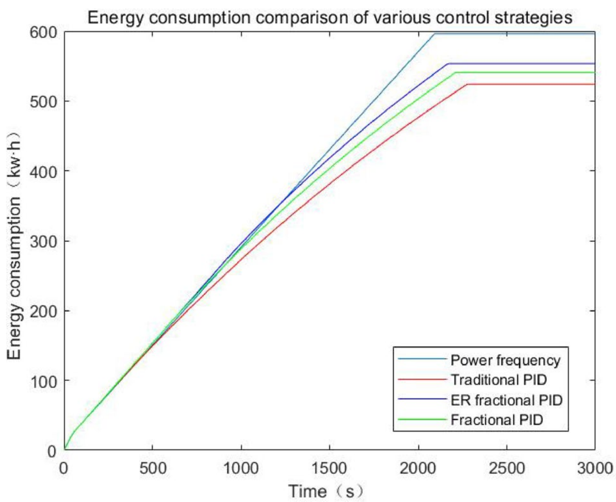

Fig. 9. Energy consumption comparison of various control strategies.

Type	time(s)	energy consumption(kW·h)	Energy saving ratio	Time reduction
Power frequency	2121.7	596.2	-	-
Traditional PID	2276.6	524.0	12.1%	-7.3%vs.PF
Fractional PID	2209.0	540.5	10.3%	-4.1%vs.PF
ER fractional PID	2169.0	553.5	7.2%	+ 2.3%vs.FPID

Table 5. Control indicators of the four control types.

Metric	Power Frequency	Traditional PID	Fractional PID	ER Fractional PID
Energy (kW·h)	596.2	524.0	540.5	553.5
Time (s)	2121.7	2276.6	2209.0	2169.0

Table 6. Comprehensive comparison of control strategies.

The variable-frequency air compressor, operated under ER fractional PID control, was found to be effective in achieving energy savings within the system. Compared with power frequency air compressors, the combined use of power frequency and variable frequency air compressors has been demonstrated to result in energy savings of 7.2%, albeit with an increase in the operating time of 47.3 s. It has been demonstrated that an optimal balance between energy savings and rapidity can be achieved. The comprehensive comparison of control strategies is shown in Table 6.

Robustness: The Power Frequency control strategy has poor robustness, the Traditional PID control strategy has fair robustness, the Fractional PID control strategy has good robustness, and the ER Fractional PID control strategy has excellent robustness.

Computational Cost: The Power Frequency control strategy has a high computational cost, the Traditional PID control strategy has a medium computational cost, the Fractional PID control strategy has a low computational cost, and the ER Fractional PID control strategy has the lowest computational cost.

Conclusion

To achieve a balance between energy consumption and operational time for the air compressor unit of the semisubmersible lifting and dismantling platform, this paper presents the design of a parameter adaptive ER fractional PID controller based on conversion transformation. To evaluate the efficacy of the aforementioned controllers in a real-world setting, the control effects of the power frequency, traditional PID, fractional PID, and ER fractional PID controllers in a rapid deballasting system were compared in a Simulink environment. The results of the simulation demonstrate that, in the context of the rapid deballasting system, the ER fractional PID controller is capable of achieving a superior balance between energy savings and rapidity. The following points represent the key findings:

(1) The relationship matrix between the control objective and the controller parameters is established by the ER rule with the objective of estimating the controller parameters in accordance with the different operational states of the air compressor. This enables a timelier and accurate control effect to be achieved.
(2) The SLP method is employed to increase the precision of the parameters of the ER rule in real time, thereby facilitating more exact estimation of these parameters and, consequently, improving the overall performance of the controller.

It should be noted that:

- Parameter optimisation relies on simulation data, and sensor noise in real working conditions may affect the accuracy of ER rule inference;
- The real-time performance of the SLP algorithm needs to be further optimised to meet higher frequency control requirements.

In conclusion, a parameter-adaptive ER fractional PID controller for the air compressors of the rapid deballasting system of the semisubmersible lifting and dismantling platform is proposed. This novel control strategy offers a better balance between energy consumption and operating time. This may be taken as a reference for the control strategy of the air compressor unit. Nevertheless, the control effect has been verified through simulation; however, the actual control effect still requires verification during the subsequent construction of the same type of semisubmersible lifting and dismantling platform.

Future work will focus on:

- Embedding online learning mechanism to enhance dynamic environment adaptability;
- Conducting hardware-in-the-loop tests on a real ship platform to verify engineering feasibility.

Compared to existing intelligent control methods, our approach achieves the first collaborative adaptive regulation of five fractional PID parameters (Kp, Ki, Kd, λ, μ) by fusing the evidential reasoning capability of

ER rules and the real-time optimization property of SLP. This novel strategy provides a better trade-off between energy consumption and operational efficiency, offering a reference for complex industrial control systems.

Data availability
The datasets generated or analyzed during this study are within the manuscript.

Received: 11 March 2025; Accepted: 21 November 2025
Published online: 28 November 2025

References
1. Saidur, R., Rahim, N. A. & Hasanuzzaman, M. A review on compressed-air energy use and energy savings. *Renew. Sustain. Energy Rev.* **14**, 1135–1153 (2010).
2. Jianda, H. et al. Simple PID parameter tuning method based on outputs of the closed loop system. *Chin. J. Mech. Eng.* **29** (03), 25–34 (2016).
3. Ristanovic, M., Cojbasic, Z. & Lazic, D. Intelligent control of DC motor driven electromechanical fin actuator. *Control Eng. Pract.* **20** (6), 610–617 (2012).
4. Karasakal, O. et al. An error-based on-line rule weight adjustment method for fuzzy PID controllers. *Expert Syst. Appl.* **38** (8), 10124–10132 (2011).
5. Yang, J. B. & Xu, D. L. Evidential reasoning rule for evidence combination. *Artif. Intell.* **205**, 1–29 (2013).
6. Zhou, J. L., Pu, Y. F. & Liao, K. The principle of fractional calculus and its application in modern signal analysis and processing. (Science Press, 2010).
7. Tepljakov, A. et al. FOPID controllers and their industrial applications: A comprehensive survey. *J. Control Autom. Electr. Syst.* **32**, 3–31 (2021).
8. Hu, S. S. Basic Course of Principles of Automatic Control. 3rd Edition. (Science Press, 2013).
9. Yang, J. B. & Xu, D. L. A study on generalizing bayesian inference to evidential Reasoning, belief Fu-nctions: theory and applications. (Springer, 2014).
10. Xiao, F. E. F. M. C. D. M. Evidential fuzzy multicriteria decision making based on belief entropy. *IEEE Tr-ansactions Fuzzy Syst.* **PP** (99), 1–1 (2019).
11. Liu, Y., Chen, Z. & Yang, J. B. Evidential reasoning for Real-Time safety assessment in autonomous systems. *IEEE Trans Ind. Inf.* **18** (5), 3021–3030 (2022).
12. Smarandache, F. et al. Fusion of sources of evidence with different importances and relia-bilities. In *2010 13th International Conference on Information Fusion.IEEE*. (2011).
13. Willis, M. J. & Von Stosch, M. LO-constrained regression using mixed integer linear programming. *Ch-emometrics Intell. Lab. Syst.* **165**, 29–37 (2017).
14. Lamberti, L. & Pappalettere, C. Move limits definition in structural optimization with sequential linear programming. *Part. II: Numer. Examples Computers & Structures*. **81** (4), 197–213 (2003).
15. Zhang, H. & Li, X. Real-Time sequential linear programming for dynamic systems: A case study on robotic control. *IEEE/ASME Trans Mechatron.* **27** (4), 2105–2114 (2022).
16. Wang, L., Zhang, G. & Zhao, Q. Energy-Optimal control of Variable-Frequency air compressors using adaptive PID strategies. *Energy Convers Manag.* **268**, 115987 (2022).
17. Kong, D., Lin, W. & Cai, M. L. Analysis on energy-saving operation of screw compressor under load/ unload operating conditions. *J. Bjing Univ. Aeronaut. Astronaut.* **38** (3), 405–409 (2012).

Acknowledgements
The authors would like to thank all the reviewers who participated in the review, as well as MJ Editor (www.mjeditor.com) for providing English editing services during the preparation of this manuscript.

Author contributions
Shouwen Pang: Writing Manuscripts. Jingxin Zhou: Formal Analysis.

Declarations

Competing interests
The authors declare no competing interests.

Additional information
Correspondence and requests for materials should be addressed to S.P.

Reprints and permissions information is available at www.nature.com/reprints.

Publisher's note Springer Nature remains neutral with regard to jurisdictional claims in published maps and institutional affiliations.